Optimizing organic photovoltaics using tailored heterojunctions: A photoinduced absorption study of oligothiophenes with low band gaps

R. Schueppel,[1] K. Schmidt,[2] C. Uhrich,[1] K. Schulze,[1] D. Wynands,[1] J. L. Brédas,[2] E. Brier,[3] E. Reinold,[3] H.-B. Bu,[3] P. Baeuerle,[3] B. Maennig,[1,*] M. Pfeiffer,[1,*] and K. Leo[1]

[1]*Institut für Angewandte Photophysik, Technische Universität Dresden, D-01062 Dresden, Germany*

[2]*School of Chemistry and Biochemistry, Georgia Institute of Technology, Atlanta, Georgia 30332-0400, USA*

[3]*Institut für Organische Chemie II und Neue Materialien, Universität Ulm, D-89069 Ulm, Germany*

(Received 25 April 2007; published 14 February 2008)

A power conversion efficiency of 3.4% with an open-circuit voltage of 1 V was recently demonstrated in a thin film solar cell utilizing fullerene C_{60} as acceptor and a new acceptor-substituted oligothiophene with an optical gap of 1.77 eV as donor [K. Schulze *et al.*, Adv. Mater. (Weinheim, Ger.) **18**, 2872 (2006)]. This prompted us to systematically study the energy- and electron transfer processes at the oligothiophene:fullerene heterojunction for a homologous series of these oligothiophenes. Cyclic voltammetry and ultraviolet photoelectron spectroscopy data show that the heterojunction is modified due to tuning of the highest occupied molecular orbital energy for different oligothiophene chain lengths, while the lowest unoccupied molecular orbital energy remains essentially fixed due to the presence of electron-withdrawing end groups (dicyanovinyl) attached to the oligothiophene. Use of photoinduced absorption (PA) allows the study of the electron transfer process at the heterojunction to C_{60}. Quantum-chemical calculations performed at the density functional theory and/or time-dependent density functional theory level and cation absorption spectra of diluted DCV*n*T provide an unambiguous identification of the transitions observed in the PA spectra. Upon increasing the effective energy gap of the donor-acceptor pair by increasing the ionization energy of the donor, photoinduced electron transfer is eventually replaced with energy transfer, which alters the photovoltaic operation conditions. The optimum open-circuit voltage of a solar cell is thus a trade-off between efficient charge separation at the interface and maximized effective gap. It appears that the open-circuit voltages of 1.0–1.1 V in our solar cell devices have reached an optimum since higher voltages result in a loss in charge separation efficiency.

DOI: 10.1103/PhysRevB.77.085311 PACS number(s): 73.50.Gr, 73.40.Lq, 84.60.Jt, 78.66.Qn

I. INTRODUCTION

Organic solar cells[1,2] have recently been investigated intensively due to their advantages such as low cost, flexibility, and short energy payback time. For a broad application of organic solar cells, a device power conversion efficiency (PCE) of 10% is considered to be necessary.[3] At present, PCE values around 4%–5% (Refs. 4–7) (including carefully optimized postproduction treatment) have been reported using heterojunctions of fullerene derivatives as acceptor and small donor molecules, e.g., copper phthalocyanine (CuPc),[8] or polymers such as polythiophene derivatives, e.g., poly(3-hexylthiophene-2,5,diyl) (P3HT).[9] P3HT:PCBM bulk heterojunction solar cells achieve an internal quantum efficiency close to unity; nevertheless, these cells still suffer from low voltage (V_{oc}=0.6V) limiting the PCE.[10] Thus, a major issue in developing efficient devices is to clarify the origin of the open-circuit voltage and its optimization.[11]

The electronic properties of polythiophenes such as P3HT[10] have proven particularly advantageous to achieve highly efficient solar cells. Recently, Scharber *et al.* characterized more than two dozen polymers acting as donor material in polymer:fullerene bulk heterojunction solar cells.[12] The open-circuit voltage of these photovoltaic cells linearly correlates with the oxidation potential measured with cyclic voltammetry [i.e., the respective highest occupied molecular orbital (HOMO) level energy]. Furthermore, Scharber *et al.* used their data to predict the donor energy levels that are required at the donor:fullerene heterojunction to reach PCE values as high as 10% by assuming optimized values of the fill factor (FF) and the external quantum efficiency. Their major observation is that the donor lowest unoccupied molecular orbital (LUMO) level should be offset by 0.3 eV with respect to the LUMO of the acceptor material,[13] while the band gap of the donor should be lower than 1.74 eV. Accordingly, with C_{60} fullerene as acceptor, a donor material with a LUMO energy between −3.5 and −3.7 eV is required. In order to (i) achieve an energetically fixed LUMO level and, at the same time, (ii) be able to modify the HOMO level energy, we have attached strong acceptor groups at the ends of the thiophene oligomers. With such acceptors, the LUMO wave function is expected to localize on the acceptor group rather than the oligomer backbone. This was demonstrated, e.g., for tricyanovinyl (TCV)-capped oligothiophenes,[14,15] where the LUMO energy is solely determined (i.e., fixed) by the strong TCV acceptor group and becomes independent of backbone modifications (such as chain length variations).

However, TCV acceptor groups stabilize the LUMO level considerably below the targeted value of −3.5 to −3.7 eV. Therefore, we have chosen to work with the dicyanovinyl (DCV) acceptor that is expected to stabilize the LUMO level to a lesser extent than TCV. Utilizing dicyanovinyl end-capped oligothiophenes (shown in Fig. 1) and varying the length of the oligothiophene *core*, we have tuned the relative position of LUMO and HOMO levels at the interface to C_{60}. Recently, we have demonstrated efficient organic solar cells incorporating an quinquethiophene derivative.[16]

In this work, we present a comparative study on a homologous series of oligothiophene derivatives, where the

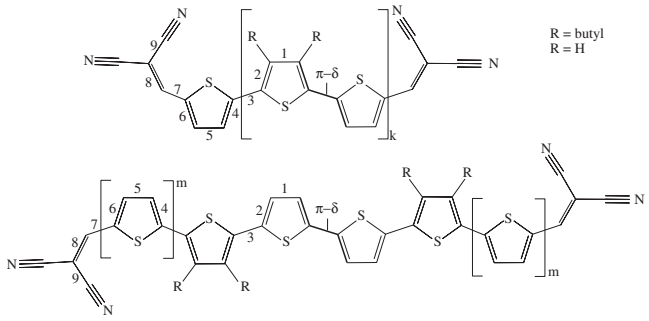

FIG. 1. Chemical structure of DCV3T ($k=1$), DCV4T ($m=0$), DCV5T ($k=2$), and DCV6T ($m=1$). Bond lengths (numbers) and dihedral angles are given in Table IV.

HOMO levels are systematically altered with the length of the molecule, while the LUMO level is almost energetically fixed. We discuss the energy levels within the DCV*n*T series as measured by cyclic voltammetry (CV) and ultraviolet photoelectron spectroscopy (UPS), followed by an investigation of the electron and energy transfer processes at the interface of DCV*n*T to fullerene by means of photoinduced absorption (PA). To allow a comprehensive interpretation of the PA spectra, both triplet-triplet and cation transitions were calculated using time-dependent density functional theory (TD-DFT). Additionally, the cation absorption spectra were recorded for dilute solutions of DCV*n*T. Finally, we compare the solar cell characteristics within the DCV*n*T series and determine the trade-off between high open-circuit voltage and efficient charge separation, which can lead to an optimized power conversion efficiency.

II. METHODOLOGY

A. Experiment

A commercial spectrophotometer (Shimadzu UV-2101/3101) is used for absorption measurements. Luminescence spectra were recorded using a FluoroMAX (Spex) with separated monochromators for excitation and luminescence light. Luminescence and absorption spectra of oligothiophenes in solution were taken in CH_2Cl_2 at room temperature.

A mechanically chopped argon ion laser (514 nm) provides the pump excitation (300 mW cm^{-2}) in PA. The probe beam provided by a tungsten-halogen white-light source was recorded in transmission geometry with either a Si or an InGaAs photodiode after passing a monochromator and detected with a lock-in amplifier. For low temperature measurements down to 10 K, the samples were kept in helium vapor in a continuous flow cryostat. As oxygen acts as a strong quencher of the C_{60} triplet state,[17] the samples are encapsulated using a cover glass glued on top. A cavity is milled into the cover glass to provide a spacing and thus avoid interference effects between the two glasses. Neat and blend layer of DCV*n*T and DCV*n*T:C_{60} were both prepared on one substrate and measured successively to achieve comparable PA intensity.

DCV*n*T was synthesized according to the route recently developed.[16,18,19] DCV3T was sublimated once and C_{60} twice by thermal vacuum gradient sublimation prior to use. DCV4T, DCV5T:C_{60} (due to the marginal amount of material available), and DCV6T (decomposition at high temperatures) were not sublimated; a partial cleaning is achieved by heating the material in the evaporation chamber slightly below its sublimation temperature for a reasonably extended time; purification is indicated by an increased pressure (degassing of impurities, approximately 10^{-6} mbar) which reduces again (approximately 30 min). The organic films are vapor deposited onto glass substrates in an ultrahigh vacuum (10^{-7} mbar) system with deposition rates of about 0.1 Å s^{-1}. The thickness is determined using a quartz crystal monitor.

Solar cells were prepared on semitransparent indium tin oxide (ITO) coated glass substrates (Thin Film Devices Inc., sheet resistance $<30\ \Omega/\mathrm{sq}$) and have an average size of 6–8 mm^2. Substrates were cleaned using detergent, acetone, and ethanol. The materials were cleaned at least twice by thermal vacuum gradient sublimation, except DCV*n*T (described above) and the dopant from Novaled AG (Dresden, Germany), used as provided.

B. Quantum chemical calculations

The photophysical properties were computed for model compounds in which the butylchains were truncated (R=H). We performed geometry optimizations for the ground state S_0 and the excited state T_1 of the neutral molecules as well as the radical-cation ground state D_0; these were followed by calculations of harmonic vibrational frequencies and normal modes in order to verify that a true minimum was reached. The S_0 state was described at the restricted density functional theory (DFT) level and the T_1 and D_0 states at the unrestricted level. The geometries of the excited singlet S_1 states were obtained from TD-DFT[20–22] calculations. In all cases, the B3LYP exchange correlation functional[23] and the split valence SV(P) basis set[24] as implemented in the TURBOMOLE package[25–27] were used; no symmetry constraints were imposed.

The vertical excitation energies were calculated using unrestricted TD-DFT, with the molecules in the fully relaxed geometry associated with S_0, S_1, T_1, or the radical ground state D_0. For the case of $T_1 \rightarrow T_n$ absorption, the initial state adopted the orbital occupation associated with T_1.

III. RESULTS AND DISCUSSION

A. Energy levels of the DCV*n*T:C_{60} donor-acceptor heterojunction

We first discuss the evolution of HOMO and LUMO levels in DCV*n*T with increasing chain length. We note that, in this paper, we loosely use expressions such as HOMO and LUMO level energies to mean ionization potentials and electron affinities. To access both quantities, CV measurements were carried out.[18] The first oxidation (E_{ox}^{onset}) and the first reduction (E_{red}^{onset}) potentials of DCV*n*T extracted from the CV measurements are shown in Table I, together with the ionization potentials (IPs) determined from UPS measurements. The onset voltage of the current peaks is determined by linearly extrapolating the slope of the respective peaks

TABLE I. Onset of first oxidation (E_{ox}^{onset}) and first reduction (E_{red}^{onset}) potentials determined from cyclic voltammetry vs Fc/Fc^+ in CH_2Cl_2 and tetrabutylammonium hexafluorophosphate (Bu_4NPF_6, 0.1*M*), 100 mV s^{-1} (Ref. 18); HOMO-LUMO levels, calculated as $E_{H,L}=-qE_{ox,red}^{onset}-E_{ref}$ (q elementary charge, ferrocene: $E_{ref}=-4.8$ eV); ionization potential (IP) from UPS; peak oxidation potential E_{ox}^0 (Ref. 18) and corresponding HOMO level E_U as suggested in Ref. 28.

	E_{ox}^{onset} (V)	E_{red}^{onset} (V)	E_H (eV)	E_L (eV)	IP (eV)	E_{ox}^0 (V)	E_U (eV)
DCV3T	0.86	−1.26	−5.66	−3.54	6.1[a]	0.98	-5.97 ± 0.18
DCV4T	0.69	−1.34	−5.49	−3.45		0.76	-5.66 ± 0.16
DCV5T	0.50	−1.40	−5.30	−3.40	5.6[b]	0.59	-5.43 ± 0.14
DCV6T	0.43	−1.36	−5.24	−3.44		0.49	-5.22 ± 0.12
C_{60}		−0.98[c]		−3.82	6.2[d]		

[a]Reference 19.
[b]Reference 16.
[c]PhMe/MeCN+Bu_4NPF_6 (0.1*M*) (Ref. 29) vs Fc/Fc^+.
[d]Reference 30.

to the voltage axis. The corresponding HOMO (E_H) and LUMO (E_L) energies, shown in Table I, are calculated using the standard expression $E_{H,L}=-qE_{ox,red}^{onset}+E_{ref}$, with $E_{ref}=-4.8$ eV the ionization energy of ferrocene and q the elementary charge.

However, it has been shown by D'Andrade *et al.*[28] that a better correspondence between HOMO values determined by UPS and CV can be achieved using the empirical formula $E_U=-(1.4\pm0.1)\times qE_{ox}^0-(4.6\pm0.08)$ eV to determine the HOMO energy from CV measurements. Here, E_{ox}^0 is determined by averaging the voltages corresponding to the peak currents of (i) oxidation of the neutral species and (ii) reduction of the oxidized species.

Along the DCV*n*T series, we observe only small fluctuations in LUMO energies indicating that the LUMO level is more or less independent of chain length. At the same time, the DCV*n*T HOMO level is significantly destabilized with every additional thiophene ring (by $\geqslant$0.15 eV for the molecules considered here).

In addition, we calculated the energies of the HOMO and LUMO levels (at the ground-state geometry) and the (gas-phase) adiabatic ionization potentials (IP_{ad}) and adiabatic electron affinities EA_{ad} for compounds DCV3T through DCV6T (Table II). The calculated values confirm a destabilization of the HOMO taking place more rapidly than the destabilization of the LUMO as the number of thienyl units increases.

We now turn to a discussion of the mutual arrangement of the DCV*n*T and C_{60} HOMO and LUMO levels. We will pay particular attention to three important quantities that characterize the DCV*n*T:C_{60} donor (D)/acceptor (A) heterojunction: (i) the LUMO level energy difference $\Delta E_L=E_L^D-E_L^A$, (ii) the HOMO level energy difference $\Delta E_H=E_H^D-E_H^A$, and (iii) the resulting effective gap $\Delta E_{DA}=E_L^A-E_H^D$ between the HOMO level of donor and the LUMO level of the acceptor. First, we focus on the experimentally well-defined DCV3T:C_{60} interface, and second, we consider the evolution of the relative position of the energy levels along the DCV*n*T series with respect to the interface to C_{60}.

The HOMO position of a C_{60} film is reported at −6.2 eV using UPS.[30] The energy (transport) gap of C_{60}, determined by inverse photoelectron spectroscopy, is reported as 2.3 ± 0.1 eV.[31] This value is in accordance with the difference between oxidation and reduction potentials determined by CV.[32] The corresponding C_{60} LUMO energy is −3.9 eV.

The electron affinity of DCV3T is found to be 0.26 eV lower than in C_{60} when comparing the photovoltage of flat heterojunction solar cells using either DCV3T or C_{60} as acceptor material.[19] This value is well reproduced by comparing the reduction potentials (see Table I) of DCV3T and C_{60} ($\Delta E_L=0.28$ eV). Thus, the LUMO of DCV3T is evaluated to be −3.62 eV.

The difference between the ionization potentials of DCV3T and C_{60}, both measured with UPS, is with 0.1 eV rather small (see Table I). The HOMO energy $E_U=-5.97\pm0.18$ eV of DCV3T derived according to the empirical formula suggested by D'Andrade *et al.*[28] from the oxidation potential E_{ox}^0 agrees within the error margins with the UPS value (−6.1 eV).[19] However, the HOMO energy ($E_H=-5.66$ eV) obtained from the onset of the oxidation potential markedly differs from both the UPS value and the value $E_U=-5.97$ eV derived from E_{ox}^0. From $\Delta E_H=0.23$ eV (resulting from the difference $E_U=-5.97$ eV of DCV3T and −6.2 eV of C_{60}) and the energy gap of C_{60} (2.3 eV), we can estimate the effective interfacial gap ΔE_{DA} as 2.07 eV.

Having characterized the heterojunction DCV3T:C_{60} based on UPS data, we are able to describe the evolution of DCV*n*T:C_{60} level offsets along the homologous series of

TABLE II. Calculated adiabatic ionization potentials and electron affinities as well as HOMO and LUMO energies (in eV).

	HOMO	LUMO	IP_{ad}	EA_{ad}
DCV3T	−6.21	−3.70	7.25	−2.68
DCV4T	−5.94	−3.56	6.87	−2.65
DCV5T	−5.72	−3.46	6.59	−2.61
DCV6T	−5.58	−3.37	6.37	−2.60

TABLE III. Vertical absorption and fluorescence transition energies (in eV) obtained for DCV*n*T in thin film and solution (CH_2Cl_2) at room temperature in comparison to the corresponding TD-DFT calculated values.

	Thin film				Solution				TD-DFT			
n	3	4	5	6	3	4	5	6	3	4	5	6
$S_0 \rightarrow S_1$	2.33	2.31	2.21	2.13	2.60	2.58	2.47	2.39	2.38	2.21	2.06	1.97
$S_1 \rightarrow S_0$	1.78	1.74	1.65	1.60	2.03	1.88	1.79	1.68	2.18	2.00	1.87	1.77

DCV*n*T on the basis of the oxidation and reduction potentials. In the following, we use the HOMO energy levels (E_U) determined from the peak oxidation potentials (E_{ox}^0). Additionally, it is assumed that the interfacial dipole and the influence of DCV*n*T on the energy levels of C_{60} are independent of the particular oligothiophene.

The LUMO level difference essentially remains constant ΔE_L=0.28 (n=3), 0.36 (n=4), 0.42 (n=5), and 0.38 eV (n=6). In strong contrast, the offset between the HOMO levels increases from ΔE_H=0.23 (n=3), 0.54 (n=4), and 0.77 (n=5) to 0.98 eV (n=6). Consequently, the effective interfacial energy gap between the DCV*n*T HOMO and C_{60} LUMO reduces with increasing chain length from ΔE_{DA}=2.07 (n=3), 1.76 (n=4), and 1.53 (n=5) to 1.32 eV (n=6).

We note, however, that these values (ΔE_H and ΔE_{DA}) should be used with care. We have already mentioned the discrepancy between UPS and CV data for DCV3T. For DCV5T, the ionization potential derived from UPS is 5.6 eV, while the HOMO level determined by the onset oxidation potential (−5.30 eV) as well as the HOMO level determined by the empirical relation suggested by D'Andrade *et al.* (-5.43 ± 0.14 eV) are considerably higher. As a rule, we find that CV consistently underestimates the ionization potential as compared to UPS. As a consequence, the interfacial gap ΔE_{DA} is underestimated as well. A possible explanation is that the oxidized state of DCV*n*T is stabilized in the CV measurement when using polar solvents such as dichloromethane as a result of the strong quadrupolar moment of DCV*n*T induced by electron withdrawing DCV groups at both ends.

Nevertheless, the experimental results clearly prove that the HOMO level steadily increases within the homologous DCV*n*T series and, consequently, that the interfacial gap of DCV*n*T:C_{60} decreases. Thus, as discussed earlier by Halls *et al.*,[33] we can expect that the larger offset of the HOMO levels between DCV*n*T and C_{60} leads to an increased driving force for dissociation of excitons into carrier pairs at the donor-acceptor interface.

B. Singlet-singlet transitions of DCV*n*T

The vertical $S_0 \rightarrow S_1$ ($S_1 \rightarrow S_0$) transition energies (shown in Table III) were estimated from the experimental spectra [Fig. 2(a)] by averaging the transition energies with the absorbance $A(E)$ or the fluorescence intensity $I(E)$, respectively,[34]

$$E_{\text{vert}}^{\text{abs}} = \frac{\int E \times A(E) dE}{\int A(E) dE}, \quad E_{\text{vert}}^{\text{em}} = \frac{\int E \times I(E) dE}{\int I(E) dE}. \quad (1)$$

The absorption (emission) energies obtained for the DCV*n*T molecules are markedly smaller than for unsubstituted or regioregular alkyl-substituted oligothiophenes [e.g., 2.6 (2.0) eV for DCV3T vs. 3.6 (2.6) eV in 3T dissolved in CH_2Cl_2].[34,35] With $S_0 \rightarrow S_1$ being well characterized as a HOMO→LUMO transition, the reduction in transition energy can be attributed mainly to the stabilization of the LUMO upon DCV substitution. Both the $S_0 \rightarrow S_1$ and $S_1 \rightarrow S_0$ transition energies exhibit a pronounced size dependence, which appears to be inversely linear with n for molecules with $n > 3$ and are strongly influenced by the environment [Fig. 2(b)].

For unsubstituted oligothiophenes (nT), the vertical transition energy in both absorption and fluorescence scales inversely with the number of double bonds N ($N=2n$ for nT) until $n > 8$ (beyond which the energies start to saturate).[34] In contrast, the chain-length dependence of the lowest singlet-singlet transition in DCV*n*T clearly does not follow a $1/N$ evolution (with $N=2n+2$ for $S_0 \rightarrow S_1$ and $N=2n+1$ for $S_1 \rightarrow S_0$, *vide infra*). The deviation from $1/N$ dependence is caused in part by the strongly accepting terminal groups. The effect of the dicyanovinyl groups is largest in the smallest molecule DCV3T and expected to level off as the molecules become longer since their electronic structure is then increasingly determined by the thiophene backbone.

The TD-DFT $S_0 \rightarrow S_1$ ($S_1 \rightarrow S_0$) transition energies (Table III) are lower than their oligothiophene counterparts.[34] The

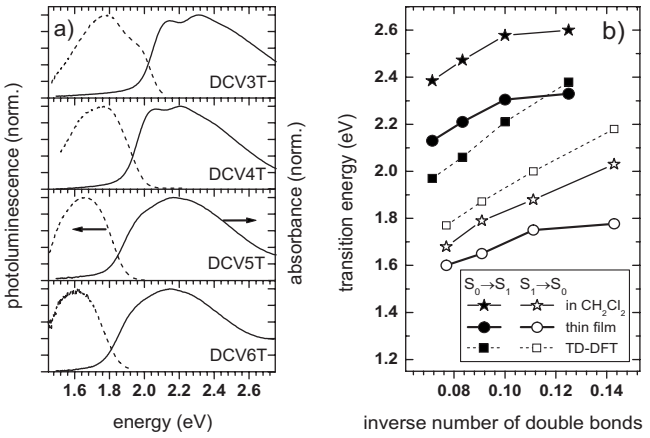

FIG. 2. (a) Absorbance [$-\log_{10}(I/I_0)$, where I is the transmitted light and I_0 is the incident light] and emission spectra of DCV*n*T thin films and (b) the vertical absorption and fluorescence transition energies (in eV) in thin films (circles) and in CH_2Cl_2 (stars) in comparison to TD-DFT calculated vertical transition energies (squares). Number of thienyl units n corresponds to $N=2n+2$ ($N=2n+1$) double bonds in the S_0 (S_1) geometry.

calculated energy difference of approximately 0.2 eV between the absorption and fluorescence transition energies is directly related to the narrowing of the HOMO-LUMO gap upon S_1 adopting a quinoidal structure (*vide supra*). The 0.2 eV TD-DFT energy difference appears to underestimate the experimental values, which range between 0.4 and 0.6 eV. Note that a precise comparison is only possible when the experimental values are extrapolated to vacuum conditions and to $T=0$ K; however, these corrections are expected to be small. Furthermore, as expected for TD-DFT calculations in general, the steepness of the $1/N$ evolution is somewhat overestimated [Fig. 2(b)] due to the inherent overestimation of long-range interactions within the method.[36] Interestingly, the departure of DCV3T from the $1/N$ dependence is almost imperceptible among the TD-DFT predicted energies.

C. Photoinduced absorption

In PA experiments, the change in transmission ΔT of the probe beam is proportional to the number of molecules that are excited by the pump beam. The recombination dynamics of the modulated excitation is separately discussed below. At low frequencies, i.e., close to steady state condition ($\omega\tau \ll 1$), the PA amplitude is proportional to the product of incident number of photons per time (pump beam), generation efficiency, and lifetime (τ) of the excited state species. Thus, such PA measurements reveal the absorption spectra specific of species that are long lived (typically microseconds to milliseconds) in accordance with the applied modulation frequency $f=\omega/2\pi$, which is typically in the range of a few hundred hertz.

The S_1 lifetime of DCVnT in a neat layer is in the nanosecond range and even drastically decreases in blends of DCVnT:C_{60}, as evidenced by a completely quenched PL of DCVnT. Thus, excited-state absorption of the DCVnT singlet state can be ruled out in standard PA spectroscopy based on mechanically chopped excitation with a kilohertz modulation frequency.

Among the potential long-lived species, transitions into the excited states of the radical anion ($D_0^- \rightarrow D_n^-$) are expected to occur in the same energy range as for the radical-cation ($D_0^+ \rightarrow D_n^+$) (Ref. 37) or triplet-triplet transitions. However, when considering the assignment of donor-type and acceptor-type molecules from the relative position of the energy levels at the DCVnT:C_{60} heterojunction, as discussed in detail above, a substantial contribution of negatively charged DCVnT is not expected. Since C_{60} is a stronger acceptor, the formation of DCVnT anions is unlikely.

As shown for mesityl-substituted nTs,[38] optical transitions due to dications are also located in the energy range investigated. However, the formation of the dication requires a mixing ratio in which the acceptor concentration largely exceeds the amount of donor molecules. The DCVnT:C_{60} blends are much less rich in C_{60} than required for a double oxidation. Therefore, the observation of dications is unlikely.

From numerous experimental studies on oligomers, such as oligophenylenes, oligophenylenevinylenes, oligothiophenes (nTs),[39,40] and various end-capped nTs,[38,41,42] it is known that the main radical-cation transition $D_0^+ \rightarrow D_n^+$ stabilizes in energy as the size of the molecules increases. The same observation has been made for $T_1 \rightarrow T_n$ in nTs.[43] The steepness with which the associated transition energies change with molecular size depends on the nature of the transition.

To provide an unambiguous assignment of the features observed in the PA spectra, quantum-chemical calculations were performed to assess the $T_1 \rightarrow T_n$ and $D_0^+ \rightarrow D_n^+$ transitions. The ordering of the main transitions of the triplet and cation species as a function of the number of thiophene units is crucial for the correct assignment.

1. Geometries

The distribution of the DFT-calculated bond lengths indicate a slightly quinoidal structure. As shown by a considerable reduction in bond-length alternation [DCV4T: 0.029 Å, $(Me)_2$4T: 0.049 Å (Ref. 38)] the DCVnT molecules adopt a more quinoidal neutral ground state than their unsubstituted counterparts. In all molecules, the deviation from planarity never exceeds 10° (Table IV). These inter-ring twists are considerably smaller than the dihedral angles found in unsubstituted nTs (20°–25.6°).[44]

Upon evolution from the neutral ground state S_0 into the excited states S_1 or T_1, or the cation ground state D_0, the double bonds expand and single bonds contract to such an extent that their character reverses with respect to the neutral ground state (Table IV). Thus, the number of double bonds decreases from $N=2n+2$ to $N=2n+1$. Since the bonds linking the thiophene rings adopt double bond character, the thiophene backbone is planarized, i.e., the torsion between the thienyl units is strongly reduced, with the reduction in inter-ring torsion being stronger in T_1 than in D_0 [DCV6T: $\delta_{cent}(S_0)=9.6°$, $\delta_{cent}(T_1)=0.2°$, $\delta_{cent}(D_0)=0.4°$] as well as in S_1 [$\delta_{cent}(S_1)=0.4°$]. The reversal in the bond-length pattern is consistent with a transition from small to strong quinoidal character.

2. Triplet and cation transitions

When monitoring the energy range below $S_0 \rightarrow S_1$, the triplet-triplet absorption $T_1 \rightarrow T_n$ and the radical cation $D_0^+ \rightarrow D_n^+$ absorption might be superimposed in the observed photoinduced transmission change. The PA signal collects all transitions between states of the same multiplicity, be they triplets or doublets on radical ions.

Before discussing the measured PA spectra, we survey which transitions can potentially arise (and their ordering) on the basis of the calculated absorption spectra. Since PA spectroscopy averages on a microsecond to millisecond time scale and thus allows for structural relaxation, the absorption spectra need to be determined in the fully relaxed geometries of either the ground state of the radical cation or the neutral T_1 state. The calculated transition energies and oscillator strengths associated with these absorption processes are collected in Table V.

Among the calculated triplet states, we find one dominant transition $T_1 \rightarrow T_4$ (DCV3T: 1.77 eV, DCV4T: 1.59 eV, DCV5T: 1.43 eV, and DCV6T: 1.30 eV) (Fig. 3). The T_1

TABLE IV. Selected bond lengths, number N of double bonds, and dihedral angles δ between thiophene rings (see Fig. 1) in different relaxed geometries (R=H). δ_{cent} refers to the dihedral angle enclosed by the two inner (or inner and adjacent) rings, while δ_{term} denotes the twist between the outermost and its neighboring ring; δ_{cent} and δ_{term} coincide in DCV3T. Deviating δ values for a structurally equivalent angle are given in parentheses.

		DCV3T			DCV4T			DCV5T			DCV6T		
		S_0	T_1	D_0^+	S_0	T_1	D_0^+	S_0	T_1	D_0^+	S_0	T_1	D_0^+
d (Å)	1	1.411	1.368	1.385	1.411	1.373	1.389	1.413	1.373	1.390	1.414	1.379	1.393
	2	1.390	1.438	1.416	1.390	1.434	1.412	1.389	1.431	1.411	1.388	1.422	1.408
	3	1.443	1.390	1.418	1.444	1.387	1.416	1.444	1.396	1.419	1.444	1.409	1.424
	4	1.395	1.428	1.441	1.395	1.418	1.405	1.396	1.413	1.401	1.396	1.404	1.399
	5	1.404	1.377	1.391	1.404	1.385	1.396	1.404	1.389	1.399	1.403	1.397	1.401
	6	1.398	1.425	1.411	1.398	1.416	1.406	1.398	1.412	1.403	1.398	1.404	1.401
	7	1.428	1.409	1.430	1.427	1.414	1.432	1.426	1.417	1.433	1.426	1.422	1.433
	8	1.377	1.395	1.378	1.377	1.390	1.376	1.378	1.387	1.374	1.378	1.382	1.374
	9	1.432	1.427	1.432	1.432	1.429	1.432	1.434	1.431	1.434	1.432	1.431	1.433
δ_{term} (deg)		0.7 (6.6)	0.1 (0.4)	0.3 (0.5)	8.6	0.1	0.3	1.0	0.7	1.1	2.5	0.5	1.3
δ_{cent} (deg)					9.6	0.2	0.1	4.7	0.5	0.7	9.6	0.2	0.4
	N	8	7	7	10	9	9	12	11	11	14	13	13

energy (at the fully relaxed geometry) is calculated to be at 1.29 (DCV3T), 1.29 (DCV4T), 1.27 (DCV5T), and 1.26 eV (DCV6T) above S_0. When considering the sequence of calculated singlet and triplet states (Table V), it is clear that both T_1 and T_2 are located below S_1. The reverse order of T_2 and S_1 has been found in unsubstituted nTs.[43]

The radical-cation exhibits two prominent transitions below $S_0 \rightarrow S_1$. The lowest transition, $D_0 \rightarrow D_1$, is located approximately 0.5–0.7 eV below $T_1 \rightarrow T_4$ (Fig. 3). The next higher significant transition, $D_0 \rightarrow D_3$, is much stronger than $D_0 \rightarrow D_1$ and located approximately 0.3 eV above the triplet transition. Thus, the calculations indicate that, in the energy range of interest and for all molecules, the triplet-triplet transition appears between two radical-cation transitions. This ordering has been experimentally observed in nTs[39,40] and other oligomeric compounds (see, e.g., Ref. 39).

The calculated $D_0 \rightarrow D_n$ transition energies are confirmed by the experimental absorption spectra of the radical cations (see Fig. 4). DCVnT, diluted in CH_2Cl_2 ($10^{-5}M$), was oxidized by adding well defined equivalents of an oxidant (thi-

TABLE V. Energies and oscillator strengths of the lowest $S_0 \rightarrow S_n$, $T_1 \rightarrow T_n$ of the neutral, and $D_0 \rightarrow D_n$ transition of the DCVnT radical-cations calculated in their fully relaxed geometry.

	DCV3T		DCV4T		DCV5T		DCV6T	
	E (eV)	f	E (eV)	f	E (eV)	f	E (eV)	f
S_0	2.38	1.635	2.20	1.993	2.17	1.810	1.97	2.436
	2.83	0.003	2.56	0.000	2.40	0.004	2.23	0.001
	3.42	0.102	3.12	0.002	2.84	0.014	2.70	0.003
	3.72	0.177	3.28	0.347	2.90	0.694	2.73	0.805
T_1	0.77	0.001	0.63	0.011	0.55	0.026	0.49	0.046
	1.76	0.023	1.44	0.000	1.21	0.016	1.04	0.016
	1.77	1.435	1.59	2.177	1.43	2.579	1.30	2.781
	2.21	0.001	1.91	0.000	1.70	0.031	1.56	0.038
	2.25	0.398	2.07	0.000	1.84	0.004	1.62	0.155
D_0	1.11	0.193	1.00	0.332	0.94	0.502	0.83	0.706
	1.79	0.000	1.57	0.000	1.45	0.001	1.27	0.000
	2.03	1.552	1.84	1.827	1.72	1.917	1.60	1.910
	2.07	0.012	1.95	0.000	1.82	0.001	1.63	0.001

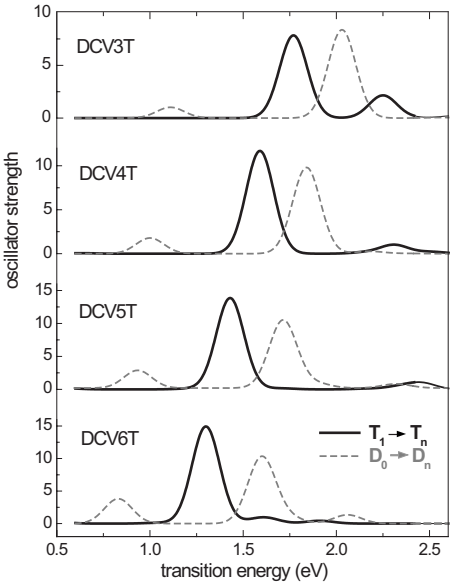

FIG. 3. Calculated $T_1 \rightarrow T_n$ (neutral molecule) and $D_0 \rightarrow D_n$ (radical-cation) absorption spectra.

anthrenium pentachloroantimonate) using a microliter injection. Thianthrenium $SbCl_5$ shows a weak absorption at 2.25 eV.[45] The vertical transition energies were obtained from the absorption spectra using Eq. (1).

The radical-cation of DCV3T is not stable; the weak feature in the corresponding absorption spectrum at 1.34 eV is attributed to $D_0 \rightarrow D_1$. For DCV4T to DCV6T, the ground-state absorption is bleached with increasing oxidation, while two infrared features build at 1.01 and 1.71 eV (DCV4T), 0.98 and 1.70 eV (DCV5T), and 0.88 and 1.63 eV (DCV6T). They can be assigned to the calculated $D_0 \rightarrow D_1$ and $D_0 \rightarrow D_3$ transitions. When the molar ratio of the oxidant exceeds 1, the DCV6T radical cation oxidizes further and a dication peak appears at 1.18 eV. Overall, the transition energies found in the experimental radical-cation spectra corroborate the positions of the $D_0 \rightarrow D_1/D_3$ TD-DFT transitions.

Thus, the calculated transition energies (see Table V) in combination with the experimental radical cation spectra (Fig. 4) allow us to identify the triplet-triplet transition as well as the cation contributions to the PA spectra, that we now discuss.

3. *Photoinduced absorption spectra of neat films of* DCV*n*T

The experimentally observed PA transitions (Fig. 5) in neat films exhibit contributions at 1.51 eV (DCV3T), 1.38 eV (DCV4T), 1.21 eV (DCV5T), and 1.12 eV (DCV6T). The film thickness is 22 nm for DCV3T, 15 nm DCV4T, 20 nm DCV5T, and 10 nm DCV6T. As we separately discuss below, the lifetime of the excited state species is approximately 50 μs for all DCV*n*T. Since the excited-state absorption of the DCV*n*T singlet state is connected to a nanosecond lifetime and photoinduced charge separation in a neat film is unlikely, we attribute these features to the $T_1 \rightarrow T_4$ triplet-triplet transitions. This assignment is confirmed by the TD-DFT calculations (see Fig. 6).

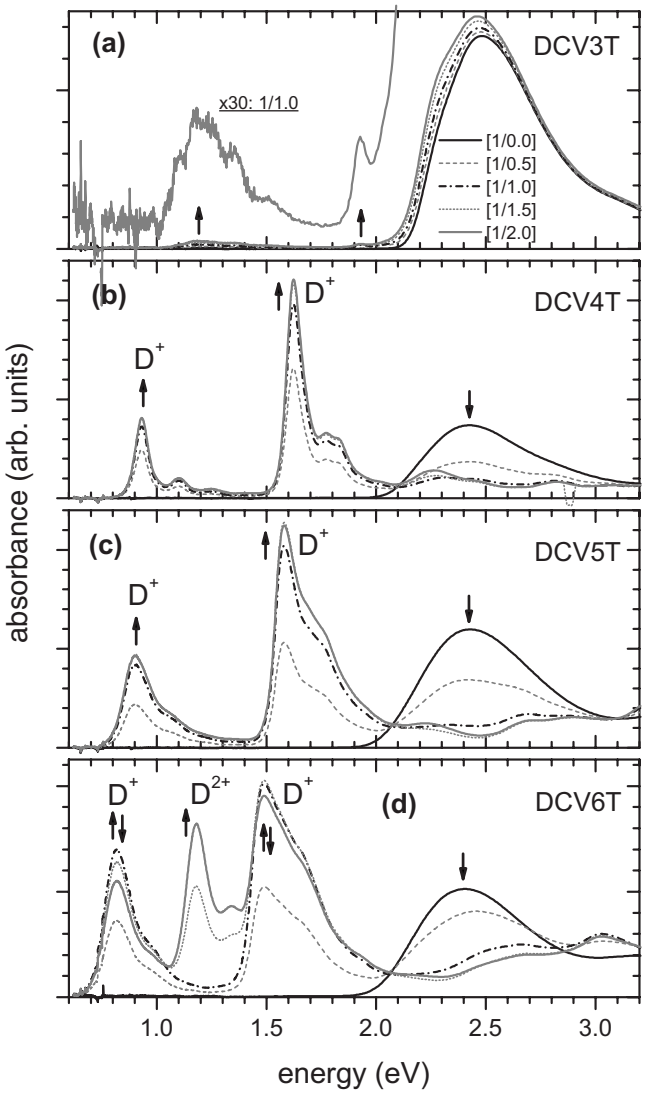

FIG. 4. Absorption spectra of chemically oxidized DCV*n*T in CH_2Cl_2 ($10^{-5}M$) by adding equivalents of thianthrenium pentachloroantimonate (0, 0.5, 1.0, 1.5, and 2.0). The arrows indicate the increase of cation (D^+) and the decrease of neutral molecule absorption with increasing oxidation. (d) For DCV6T the cation (D^+) is oxidized further, if the molar ratio of the oxidant exceed 1 and the absorption of dications (D^{2+}) appear.

4. *Photoinduced absorption spectra of* DCV*n*T:C_{60} *blends*

In blends with C_{60}, the total amount of DCV*n*T was kept constant compared to the neat layer while we dope DCV*n*T by fullerene C_{60} in a molecular 1:1 ratio. The DCV*n*T triplet exciton contribution to the PA spectra is still present and, remarkably, even increases in DCV3T:C_{60}, DCV4T:C_{60}, and DCV5T:C_{60} with respect to the neat layers.

The frequency dependence of the triplet transition is similar to the single layer and result in the same lifetime, *vide infra*. Thus, the increased PA amplitude at low modulation frequencies ($\omega\tau \ll 1$) in the blend layer in Fig. 5 corresponds to an increased generation efficiency of the triplet state compared to the single layer.

The emerging cation transitions which occur as a result of exciton dissociation at the donor-acceptor heterojunction are

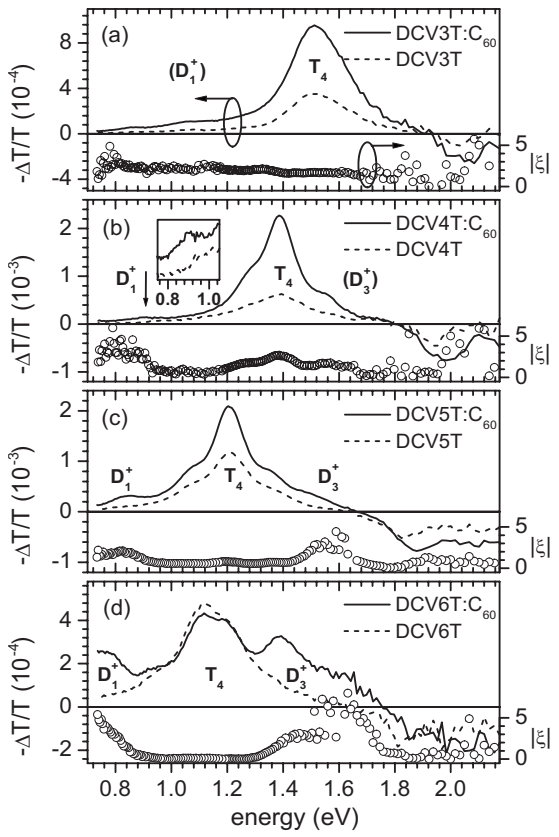

FIG. 5. Photoinduced absorption spectra of (a) DCV3T and DCV3T:C_{60}, (b) DCV4T and DCV4T:C_{60}, (c) DCV5T and DCV5T:C_{60}, and (d) DCV6T and DCV6T:C_{60}. Open circles: absolute value $|\xi|$ of the spectral difference between neat $(-\Delta T_n/T_n)$ and blend $(-\Delta T_b/T_b)$ layer PA [see Eq. (2)]. Spectra are measured at low temperatures ($T=10$ K) and low modulation frequencies ($f=225$ Hz). D_1, D_3, and T_4 indicate the identified cation and triplet transitions; transitions in brackets indicate the expected spectral position.

monitored by the relative difference of blend $(-\Delta T_b/T_b)$ vs neat $(-\Delta T_n/T_n)$ layer PA,

$$\xi = (\Delta T_b/T_b - \Delta T_n/T_n)/(\Delta T_n/T_n). \tag{2}$$

In the DCV3T:C_{60} blend, we find the PA spectrum to be essentially similar to that of the neat layer ($\xi \approx$ const) with an increased contribution of the DCV3T triplet transition ($\xi=1.73$ at 1.51 eV). Tiny contributions of the blend PA spectrum [Fig. 5(a)] in the infrared region at 0.84 and 1.04 eV might be assigned to cation contributions (calculated value: 1.11 eV, see Table V), although the relative difference ξ of blend and neat layer is almost constant and, therefore, the fraction of generated cations is negligible.

The same situation is observed in blend layers of DCV4T and C_{60}, with the triplet transition at 1.38 eV increasing ($\xi=2.61$). A significant contribution at 0.90 eV occurs [see inset of Fig. 5(b)] that we attribute to the cation transition of DCV4T, calculated at 1.00 eV.

When comparing the PA of DCV5T:C_{60} blend and DCV5T neat layers, significant differences are observable at 0.83 and 1.54 eV, as well as a slightly increased triplet contribution at 1.21 eV ($\xi=0.77$). We assign the PA transitions at 0.83 and 1.54 eV induced by the admixture of C_{60} to the cation transitions $D_0 \rightarrow D_1$ (calculated value: 0.94 eV) and $D_0 \rightarrow D_3$ (1.72 eV) of DCV5T.

Blending DCV6T and C_{60} reveals more pronounced differences in the PA spectra with cation transitions arising at 0.75 and 1.39 eV. The triplet contribution at 1.10 eV is still present, but decreases ($\xi=-0.10$).

Thus, we can assign the features experimentally observed at 1.51 eV (DCV3T), 1.38 eV (DCV4T), 1.21 eV (DCV5T), and 1.12 eV (DCV6T) to triplet-triplet transitions (see Fig. 6). Additional features at 0.90 eV (DCV4T), 0.83 and 1.54 eV (DCV5T), and 0.75 and 1.39 eV (DCV6T) correspond to cation transitions.

With exciton dissociation and charge carrier separation, a C_{60} anion contribution to the spectra is expected in addition to the DCVnT cation. In solution, C_{60}^- transition energies are reported at 1.15 eV and weaker at 1.30 eV,[46–49] as well as less significant contributions in the visible range.[46,50] In thin films of oligothiophene:fullerene blends, a tiny contribution of C_{60} anions is observed at 1.17 eV.[51] This transition energy is in the same range as the much more intense triplet contributions in DCV5T and DCV6T; thus, we have no access to the fullerene anion in our spectra.

On the basis of these assignments, we observe that the transition energies do not strictly follow a $1/N$ relationship (Fig. 6), which is consistent with the theoretical results.[52] As argued earlier in the case of $S_0 \rightarrow S_1$ ($S_1 \rightarrow S_0$) transitions, we attribute the marked deviation in the case of DCV3T to the strong influence of the C-$(CN)_2$ groups in this molecule.

5. Recombination dynamics

In the following, we discuss the recombination dynamics of the DCVnT triplet excitons as well as the DCV6T cation. We consider both cases of purely monomolecular (MR) and purely bimolecular (BR) recombination,

$$\frac{dn}{dt} = G(t) - \frac{n}{\tau_{\mathrm{MR}}} \quad \text{and} \quad \frac{dn}{dt} = G(t) - \beta n^2, \tag{3}$$

respectively, where the excited state species density $n(t)$ is generated by the pump light $G(t)=g[\cos(\omega t)+1]$. Here, we use $g=\eta I_p$, where η is the generation efficiency of the excited state and I_p is the pump intensity. The modulation frequency f is represented by $\omega=2\pi f$.

The PA amplitude is proportional to the oscillating excited state population density[53] n_s. For MR, the amplitude is given by[54]

$$n_s = \frac{g\tau_{\mathrm{MR}}}{\sqrt{1+\omega^2\tau_{\mathrm{MR}}^2}}. \tag{4}$$

For BR, Eq. (3) is solved using a symmetric square light wave approximation.[54] Thus, the PA amplitude is proportional to

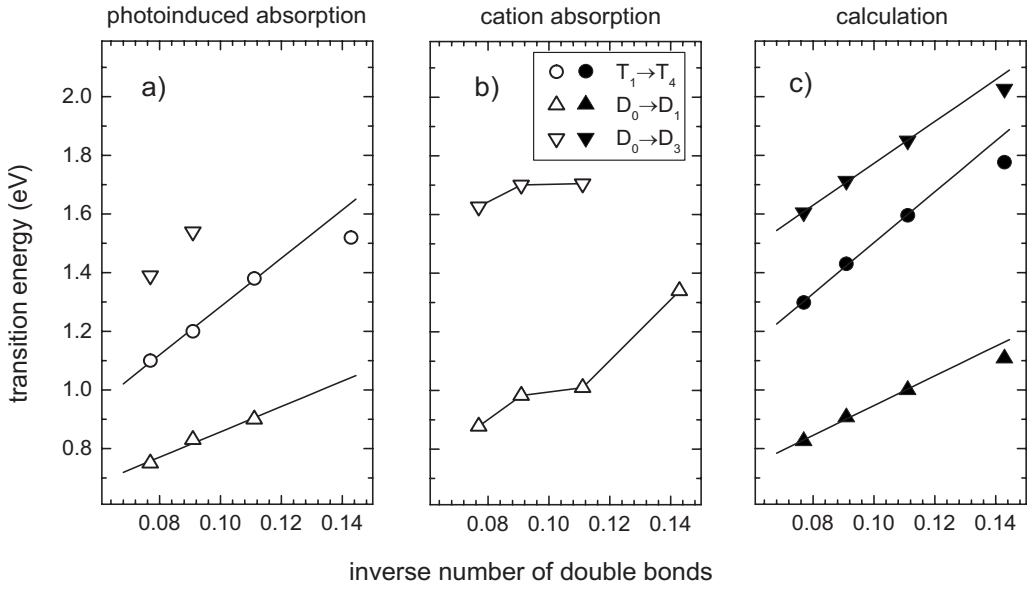

FIG. 6. Energies of the main transitions in the triplet manifold of the neutral molecule and doublet manifold in the radical cation as a function of the molecular size, extracted from (a) photoinduced absorption of thin films, (b) absorption spectra in thianthrenium $SbCl_5$, and (c) TD-DFT calculations.

$$n_s = g\tau_{\mathrm{BR}} \frac{\alpha \tanh \alpha}{\alpha + \tanh \alpha}, \tag{5}$$

where $\alpha = \pi/(\omega\tau_{\mathrm{BR}})$. The bimolecular lifetime[54] τ_{BR} is defined as $n_s = g\tau_{\mathrm{BR}}$ under steady-state conditions and depends on the pump intensity, $\tau_{\mathrm{BR}} = 1/\sqrt{g\beta}$. We note that another approach is given by a series expansion[55] of $n(t)$.

In Fig. 7, the frequency dependence of the PA amplitude $[-\Delta T/T](\omega)$ is given for neat and blend layers of DCVnT and DCVnT:C_{60} at the respective triplet transition energies (see Table VI). For DCV6T:C_{60}, the recombination dynamics of both DCV6T cation transitions are shown, too. For DCV5T and DCV4T, the cation transition is superimposed by the triplet transition background (see Fig. 5) and thus analyzing the lifetime of the cation might be misleading.

The lifetime of the respective DCVnT triplet and cation is obtained by a fit according to Eq. (4) for monomolecular recombination (τ_{MR}) and to Eq. (5) for bimolecular recombination (τ_{BR}). The values are summarized in Table VI. The lifetime τ_{BR} is in the same order of magnitude as τ_{MR}, albeit slightly larger. Moreover, the fit quality of $[-\Delta T/T](\omega)$ is slightly superior when assuming the bimolecular model. Nevertheless, we get *independent* of the assumed recombination model a similar $[-\Delta T/T](\omega)$ dependence and, thus, similar neat and blend layer triplet lifetimes. It is, therefore, not necessary to actually distinguish between monomolecular and bimolecular recombinations, which would require an analysis of $[-\Delta T/T](\omega)$ at different pump intensities.

For neat layers of DCVnT, the triplet lifetime ranges around 50 μs; this was confirmed for DCV3T by transient absorption.[56] The lifetime of the probed excited state is orders of magnitude higher than the lifetime of the singlet excitation (nanosecond range) and provides, thus, the justification to interpret the peak in the neat layer PA spectra as

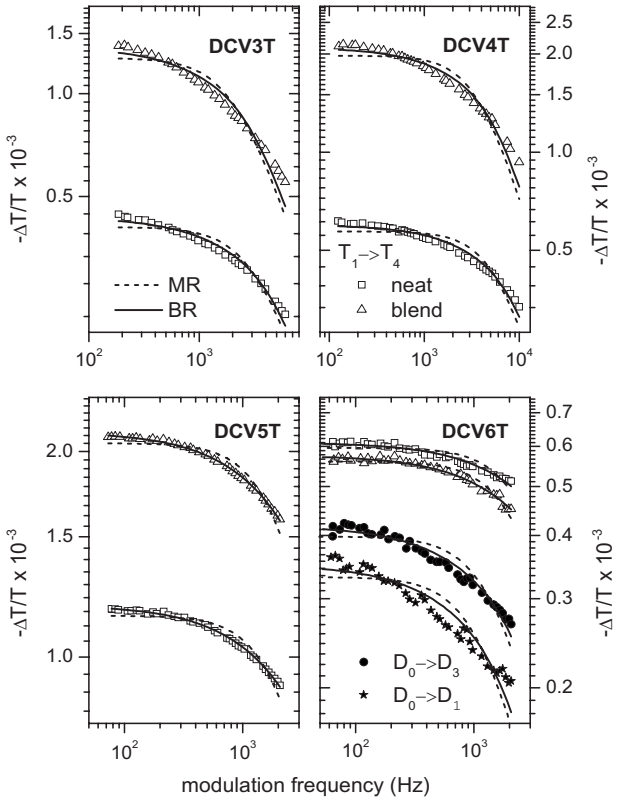

FIG. 7. Modulation frequency dependence of triplet-triplet absorption at 1.51 eV (DCV3T), 1.38 eV (DCV4T), 1.21 eV (DCV5T), and 1.12 eV (DCV6T). Rectangles: neat layer of DCVnT. Triangles: DCVnT:C_{60} blend layer. Fit according to Eq. (4) for monomolecular recombination (MR) and Eq. (5) for purely bimolecular recombination (BR). DCV6T cation absorption at 0.78 eV (stars) and 1.38 eV (circles) for DCV6T:C_{60} blend. $T = 10$ K, pump intensities correspond to Fig. 5.

TABLE VI. Left part: lifetime τ of DCVnT triplet and DCV6T cation in neat and blend layers according to a fit of the frequency dependence of the PA amplitude in Fig. 7 to Eq. (4) for monomolecular recombination (MR) and to Eq. (5) for bimolecular recombination (BR). The respective transition energies correspond to the maxima of the PA spectra in Fig. 5. Right part: calculated ratio of lifetime τ and ratio of amplitude $G=\eta I_p$ between DCVnT:C_{60} blend (b) and DCVnT neat (n) layer with respect to MR and BR recombinations.

Sample	Energy (eV)	τ_{MR} (μs)	τ_{BR} (μs)		τ_b/τ_n	g_b/g_n
DCV3T	1.51	48.0	71.7	MR	1.51	2.07
DCV3T:C_{60}	1.51	72.6	112	BR	1.56	2.02
DCV4T	1.38	27.1	38.0	MR	1.51	2.29
DCV4T:C_{60}	1.38	40.9	60.2	BR	1.58	2.21
DCV5T	1.21	67.1	76.0	MR	1.05	1.70
DCV5T:C_{60}	1.21	70.7	83.0	BR	1.09	1.64
DCV6T	1.12	53.9	53.0	MR	1.18	0.80
DCV6T:C_{60}	1.12	63.5	67.2	BR	1.27	0.74
DCV6T:C_{60}	1.38	102	142			
DCV6T:C_{60}	0.78	131	190			

absorption of the T_1 triplet state. In blend layers of DCVnT:C_{60}, we find basically the same lifetime of the DCVnT triplet. As indicated in Table VI, the ratio of blend and neat layer triplet lifetimes τ_b/τ_n ranges between 1.5 and 1.0 for all DCVnT. Considering this lifetime ratio, the difference between monomolecular and bimolecular recombinations is negligible. We want to stress that the small difference between the triplet lifetime of neat and blend layers is not sufficient to explain the different amplitudes in the steady-state PA spectra (see Fig. 5), where $\xi+1$ ranges between 3.6 and 0.9. In particular, for DCV6T, the steady state PA amplitude of the triplet transition (1.21 eV) is decreased in the blend layer $(\Delta T_b/T_b)/(\Delta T_n/T_n)=\xi+1=0.9$, while the triplet lifetime is slightly increased, $\tau_b/\tau_n \approx 1.2$.

Thus, the ratio of the generation efficiency g_b/g_n has to be considered as the more important quantity to explain the ratio of PA amplitudes (Table VI). We note that the ratio g_b/g_n reflects the generation efficiency since the pump intensity as well as absorbance of the neat and blend layers were kept equal. The absorption of fullerene C_{60} at 514 nm is negligible, and the material amount of DCVnT was equal between blend and neat layers. Due to a molecular ratio of close to 1:1 in the blend layer, the exciton density is decreased by a factor of 2, which might in general influence the bimolecular recombination. Although, the difference between monomolecular and bimolecular recombination in g_b/g_n is negligible.

We find a noticeable consistency between the ratio of triplet generation efficiency g_b/g_n and the ratio of the blend and neat layer transition amplitudes in the steady-state PA spectra indicated by $\xi+1$. In particular, for DCV6T, the decrease of the generation efficiency g_b/g_n exceeds the increase of the lifetime τ_b/τ_n, and thus, the ratio of the steady-state triplet exciton density that is reflected by the PA amplitude ratio $(\xi+1)$ at low frequencies $(\omega\tau<1)$ is decreased. Apart from DCV3T, we find a systematic decrease of the generation from DCV4T to DCV6T. The deviant behavior of DCV3T is an additional indication of the different mechanisms that lead to the indirect triplet population, as we will discuss below.

In summary, we find a similar lifetime for neat and blend layer triplet excitons, and thus, the DCVnT triplet state is unquenched for all DCVnT:C_{60}. In contrast, the generation efficiency of the triplet excitons depends on the oligothiophene chain length and systematically decreases from DCV4T to DCV6T, while DCV3T deviates from this correlation.

D. Electron versus energy transfer

The exciton dissociation ability of the DCVnT:C_{60} interface, and, therefore its ability to trigger charge carrier separation increases from DCV3T to DCV6T due to an enlarged offset of the HOMO levels between DCVnT and C_{60}. On the basis of this correlation between the efficiency of charge carrier generation and the size of the donor molecule, we now discuss the competition between DCVnT triplet vs charge carrier formation.

The PL of DCVnT is rapidly quenched in the blend. In DCV3T:C_{60} blends, only a few charge carriers below our detection limit might be generated, while the triplet generation is strongly enhanced. This increase is attributed to an indirect population of the lowest triplet state via the following pathway:[56] (i) singlet-singlet energy transfer from DCV3T to C_{60} (whose fast rate was demonstrated by sensitized emission of C_{60}), (ii) highly efficient intersystem crossing (ISC) on C_{60}, and (iii) subsequent triplet energy transfer back to DCV3T. The same sequence of energy-transfer processes (i)–(iii) is found in mixtures of oligothienylenevinylenes (nTVs) with a fullerene derivative (MP-C_{60}) in a nonpolar solvent (toluene),[57] resulting in an indirectly populated triplet state of nTV.

However, for DCVnT with $n \geqslant 4$, sensitized emission of C_{60} is not observed, indicating that singlet-singlet transfer between donor and acceptor species does not occur. The appearance of cation transitions in the PA spectrum is evidence for the generation of charge carriers in DCVnT:C_{60} ($n \geqslant 4$) blends. Consequently, we attribute the PL quenching to electron-hole separation at the DCVnT:C_{60} ($n \geqslant 4$) donor-acceptor interface.

Simultaneously, an increased triplet population was observed for DCV4T (ξ=2.61) and DCV5T (ξ=0.77). In DCV6T:C_{60} (ξ=−0.10), the triplet population is smaller compared to the pristine DCV6T layer, but present. In the absence of sensitized C_{60} emission, the observed triplet population cannot be explained by indirect population of T_1 of DCVnT ($n \geqslant 4$) from the lowest triplet state of C_{60}. Rather, the triplet generation is mediated by relaxation of an interface donor-acceptor charge transfer state DCVnT$^+$:C_{60}^-; this is reminiscent of the mechanism described by Ford *et al.* for polyfluorene:PFB blends:[58] (i) after exciting the donor D, charge carriers are separated at the interface, forming a $^1D^+A^-$ singlet charge-transfer state at the interface; (ii) efficient conversion of the singlet into the triplet species of D^+A^- via ISC (due to small exchange interaction); and (iii) relaxation of $^3D^+A^-$ into the lower-lying donor T_1. The temperature dependence of the DCV5T PA spectrum between 1.1 and 1.6 eV reveals a total PA amplitude that decreases with increasing temperature, while the ratio of cation (1.5 eV) to triplet (1.24 eV) transitions increases.[59] This indicates a thermally activated dissociation into free electron and holes, presumably within step (i) or (ii).

Indirect triplet population was also observed by Veldmans *et al.* when comparing blends of MDMO-PPV with a cyano-containing acceptor polymer (PCNEPV)[60] or with bodipy dyes[61] to pristine MDMO-PPV. The enhancement in triplet population was explained by these authors as due to a recombination of free charge carriers generated after exciton dissociation. Thus, the observation of triplet state is recognized as a loss mechanism for high open-circuit voltage polymer photovoltaic devices.

In our systems, the indirect population of the triplet state (indicated by ξ) decreases with increasing number of thienyl units from DCV4T to DCV6T. At the same time, the amplitude of the cation transition within the PA spectrum (see Fig. 5) increases along the series DCVnT:C_{60} ($n \geqslant 4$) with respect to the amplitude of the triplet transition of the neat layer. This points toward an increasing cation population, considering that the ratio of calculated oscillator strengths (see Table V) between the cation transition ($D_0 \rightarrow D_1$) and the triplet transition ($T_1 \rightarrow T_4$) remains roughly constant (0.13, 0.15, and 0.19 for DCV4T, DCV5T, and DCV6T).

The observed increase in cation population ($\propto \eta\tau$) with molecular size has to be attributed to a chain-length dependence of either the generation efficiency η or the lifetime τ of the cation. We note that an unambiguous assignment of either η or τ is not possible here since the signals of the cations are strongly superimposed in DCV4T and DCV5T by the respective triplet transition. Nevertheless, the role of η and τ can be discussed within two scenarios.

In the first scenario, we assume a constant generation efficiency η. Thus, the lifetime τ of the cation needs to increase from DCV4T to DCV6T to explain the increasing cation population. An increasing lifetime could originate from a decreasing recombination efficiency of the cation into the triplet state. This consideration is, therefore, in agreement with the decreasing indirect triplet population indicated by $\xi(n)$.

In the second scenario, we assume a constant lifetime τ while η needs to increase. Since the PL of DCVnT:C_{60} ($n \geqslant 4$) is completely quenched, the efficiency of the quenching process is near unity and therefore roughly constant within the series. Consequently, in the simple picture of a charge-separated state populated directly from the quenched singlet excitons and monitored in the PA spectra, an increasing generation efficiency of the cation is not achieved. However, if we assume an intermediate state (D^+A^-) between DCVnT and C_{60} that either recombines into a triplet state or dissociates into free charge carriers observable in PA with rate constants depending on the chain length, this scenario becomes possible.

The dissociation probability of the geminate pair was considered by Arkhipov *et al.*[62] in the case of an extended polymer in the presence of an array of acceptor molecules. Considering small-sized molecules, such a discussion needs to be extended to be able to establish a relationship between dissociation rate and donor chain length.

In summary, we observe an increasing charge carrier generation associated with a decreased indirect triplet state population for molecules DCV4T to DCV6T. This observation is consistent with the expectation from the relative positions of the energy levels at the DCVnT:C_{60} interface, as discussed in the previous section.

E. Solar cell application

In the following, we discuss the impact of the charge carrier vs triplet state generation in the DCVnT ($n \geqslant 4$) series on the photovoltaic performance. In doing so, we recognize the trade-off between efficient charge carrier separation and a high open-circuit voltage of the solar cell.

The open circuit voltage V_{oc} of polymer:PCBM solar cells was found to follow the empirical relation $eV_{oc}=\Delta E_{DA}-0.3$ eV,[12] where e is the elementary charge. Thus, a direct consequence of the reduced interfacial gap ΔE_{DA} is a reduced V_{oc} with increasing chain length.

To connect the performance of our DCVnT:C_{60} heterojunctions to the $V_{oc}(\Delta E_{DA})$ relationship, we prepared three comparable solar cells having the following layer sequence: ITO/Au (1 nm)/HTL/donor (10 nm)/C_{60} (40 nm)/4,7-diphenyl-1,10-phenanthroline (BPhen) (6 nm)/Al (100 nm), where the donor is either DCV4T (cell A), DCV5T (cell B), or DCV6T (cell C). HTL denotes a p-type hole transport layer sequence consisting of p-doped 4,4′,4″-tris(2-naphthylphenylamino)-triphenylamine (TNATA) (30 nm)/p-doped N,N'-di(naphthalen-1-yl)-N,N'-diphenyl-benzidine (α-NPD) (10 nm)/intrinsic α-NPD (5 nm). As dopant, we use the proprietary acceptor dopant NDP2 purchased from Novaled AG (Dresden, Germany) with doping ratios of 2.5 mol % for TNATA and 20 mol % for α-NPD. The p-type doping of

TABLE VII. Solar cells with layer structure ITO/Au (1)/pTNATA (30)/pNPD (10)/NPD (5)/donor (10)/C_{60} (40)/Bphen (6)/Al (100): open circuit voltage V_{oc}, short circuit current j_{sc}, and fill factor at nominally 130 mW/cm^2 simulated sunlight. For efficiency calculation, a spectral mismatch factor of approximately 0.7 needs to be taken into account. Values in parentheses refer to layer thicknesses.

Cell	Donor material	V_{oc} (V)	FF (%)	j_{sc} (mA/cm^2)	$j_{-1\ \mathrm{V}}/j_{sc}$
A	DCV4T	1.13	27.6	5.9	1.32
B	DCV5T	1.00	50.6	11.4	1.10
C	DCV6T	0.93	46.0	7.7	1.15

the transport layer increases the conductivity and improves the contact behavior;[63,64] the doping effect using NDP2 is comparable to tetrafluorotetracyanoquinodimethane (F_4-TCNQ).[16] However, the Novaled dopant is used because of its higher sublimation temperature and is therefore much easier to handle in high vacuum. The general advantages of the doping approach have been discussed earlier.[65–67] A detailed discussion on the influence of the doped HTL on the performance of this type of solar cells incorporating DCV5T have been given in Ref. 16. BPhen acts as an exciton blocker, while deposition of aluminum on top of BPhen introduces defect states enabling electron transport between C_{60} and aluminum, as suggested for the closely related material bathocuproine.[68] Table VII summarizes the specific parameters of these cells.

As discussed in Sec. III A, the interfacial energy gap ΔE_{DA} between the DCVnT (donor) HOMO and the fullerene (acceptor) LUMO reduces with the number of thienyl units n from $\Delta E_{DA}=1.76$ ($n=4$) and 1.53 ($n=5$) to 1.32 eV ($n=6$). The difference between $n=4$ and $n=5$ [$\delta(\Delta E_{DA})=0.23$ eV] as well as between $n=5$ and $n=6$ [$\delta(\Delta E_{DA})=0.21$ eV] is determined by the offset of the corresponding HOMO levels (see Table I). The decrease in interfacial gap is in accordance with the drop in open-circuit voltage V_{oc} (see Table VII): $\delta(V_{oc})=0.13$ V from $n=4$ to $n=5$ and $\delta(V_{oc})=0.09$ V between $n=5$ and $n=6$. As a best fit, we find the linear relation $eV_{oc}=0.46\times\Delta E_{DA}-0.32$ eV. The prefactor of 0.5 is related to the uncertainty induced by fitting just three samples, while Scharber *et al.* used 26 (scattering) values; however, we recover the same trend as these authors.

The FF and, in particular, the saturation factor $j_{-1\ \mathrm{V}}/j_{sc}$ (SF) provide a measure for the efficiency of charge carrier separation at the DCVnT:C_{60} interface; a small SF (ideally 1) corresponds to an efficient separation at zero bias voltage. For DCV4T (cell A), the SF (1.32) is far away from the ideal case (1.0); thus, the dissociation of charge carriers is field dependent. For cells B and C, we find reasonably well optimized solar cells as indicated by SF as well as FF. Since the DCVnT samples in the solar cells were used as provided, i.e., not purified by vacuum gradient sublimation (due to marginal amount of material), the small differences are presumably caused by different material purity grades which has a strong influence on the device performance.[69]

The current-voltage characteristics (see Fig. 8) of cell B

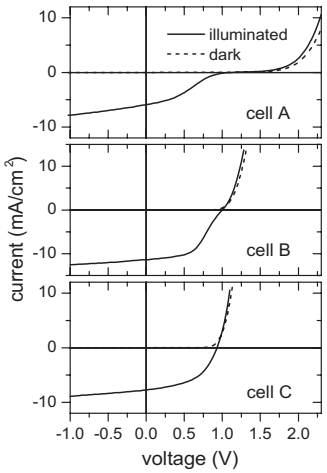

FIG. 8. *IV* characteristics of solar cells described in Table VII with donor material: (A) DCV4T, (B) DCV5T, and (C) DCV6T. Illumination was 130 mW/cm^2 simulated sunlight, a spectral mismatch of approximately 0.7 has to be considered.

(DCV5T) show a slight S-shape behavior, which is strongly increased for cell A (DCV4T). The high voltage required to drive a forward current results from a hole-injection barrier between NPD and DCVnT. The probability to overcome such a barrier is described by Staudigel *et al.*[70] Assuming a certain width of density of states (DOS), i.e., a Gaussian-broadened HOMO level, the thermally assisted hopping over the barrier is determined by the overlap of the DOS associated with the adjacent layers; these DOSs are connected by a Boltzmann term incorporating the barrier height. Therefore, a step of 0.23 eV [$\exp(-0.23eV/kT)\approx 10^{-4}$] in the HOMO level between DCV5T (cell B) and DCV4T (cell A) strongly influences the transfer probability between the HTL and the DCVnT donor.

Turning back to our earlier question on higher open-circuit voltages in organic solar cells, we conclude that we have demonstrated a solar cell (cell B, DCV5T) with a voltage close to maximum for this type of thiophene:fullerene based flat heterojunction solar cells. Inducing a higher interfacial gap ΔE_{DA} via reducing the number of thienyl units should lead to a higher open-circuit voltage according to Scharber *et al.* In DCV4T:C_{60}, we find a reduced dissociation of electrons and holes and simultaneously an increased population of the triplet state. In DCV3T:C_{60}, we actually replace the dissociation into electron and holes at the interface with an energy transfer across the interface causing the absorbed energy to be stored in triplet states.[19,56]

A mode of operation similar to our DCV5T:C_{60} solar cell, i.e., efficient charge separation accompanied by small losses due to triplet formation, has been also observed using polymer donor:acceptor blends.[60]

IV. CONCLUSION

We systematically studied the energy and electron transfer processes at a donor:C_{60} heterojunction along a homologous series of oligothiophene derivatives serving as donors. We

demonstrated with the help of CV and UPS measurements that by attaching dicyanovinyl terminal groups, the electronic properties of the oligothiophenes were tailored to maintain an almost constant LUMO energy offset of 0.3–0.5 eV to the acceptor C_{60}, while at the same time being able to steadily tune their ionization potential by the backbone size. The consequences of the altered arrangement of the energy levels at the DCVnT:C_{60} heterojunction were probed with photoinduced absorption. The energy of the anticipated transitions, i.e., triplet-triplet and cation transitions, were well predicted by TD-DFT calculations and confirmed by cation absorption spectroscopy.

With the gradual increase in effective energy gap of the donor-acceptor pair observed when going from DCV6T through DCV3T, the photoinduced electron transfer becomes replaced with energy transfer. We also observed indications that different mechanisms lead to donor triplet formation. While for DCVnT ($n \geqslant 4$) the population of the donor triplet state presumably occurs via ISC of a charge transfer state at the interface, the DCV3T T_1 state was formed after subsequent energy transfer from DCV3T S_1 across the singlet and triplet manifold of the acceptor.[56]

These effects alter the operation conditions of photovoltaic devices based on these heterojunctions. In the case of DCV5T, triplet formation constitutes only a small loss factor. In contrast, at the DCV3T:C_{60} interface, triplet state population largely exceeds charge carrier formation; thus, in such a solar cell, additional mechanisms are required to dissociate the lowest triplet state.[56]

In order to optimize the solar cell device performance, a high open-circuit voltage as well as a reasonable charge separation efficiency is required. Within our series of oligothiophenes, we find a reasonable compromise between open-circuit voltage, short-circuit current, and saturation factor by using DCV5T:C_{60} solar cells. Increasing the open-circuit voltage by using DCV4T leads to a decreased charge separation that was indicated by the saturation factor as well as by the photoinduced absorption spectra. The decreased charge carrier signature as well as the increased indirect triplet generation for DCV4T point toward a fundamental process of triplet recombination, which might be of general interest in the design of high open circuit voltage devices.[59] Using DCV6T decreases the open-circuit voltage of the device while an increase of the short circuit current or an further decrease of the saturation factor is not obtained.

ACKNOWLEDGMENTS

Financial support by the German Federal Ministry for Education and Research BMBF (Innoprofile) and the Deutsche Forschungsgemeinschaft (Leibniz) is gratefully acknowledged. The work at Georgia Tech has been partly supported by the National Science Foundation (through the STC Program under Award No. DMR-0120967 and the CRIF Program under Award No. CHE-0443564) and the Office of Naval Research.

*Present address: Heliatek GmbH, Dresden, Germany.

[1] C. W. Tang, Appl. Phys. Lett. **48**, 183 (1986).
[2] G. Yu, J. Gao, J. C. Hummelen, F. Wudl, and A. J. Heeger, Science **270**, 1789 (1995).
[3] C. J. Brabec, J. A. Hauch, P. Schilinsky, and C. Waldauf, MRS Bull. **30**, 50 (2005).
[4] J. Xue, B. P. Rand, S. Uchida, and S. R. Forrest, Adv. Mater. (Weinheim, Ger.) **17**, 66 (2005).
[5] G. Li, V. Shrotriya, J. S. Huang, Y. Yao, T. Moriarty, K. Emery, and Y. Yang, Nat. Mater. **4**, 864 (2005).
[6] P. Schilinsky, C. Waldauf, and C. J. Brabec, Adv. Funct. Mater. **16**, 1669 (2006).
[7] Y. Kim *et al.*, Nat. Mater. **5**, 197 (2006).
[8] P. Peumans, A. Yakimov, and S. R. Forrest, J. Appl. Phys. **93**, 3693 (2003).
[9] F. Padinger, R. S. Rittberger, and N. S. Sariciftci, Adv. Funct. Mater. **13**, 85 (2003).
[10] P. Schilinsky, C. Waldauf, and C. J. Brabec, Appl. Phys. Lett. **81**, 3885 (2002).
[11] C. J. Brabec, A. Cravino, D. Meissner, N. S. Sariciftci, T. Fromherz, M. T. Rispens, L. Sanchez, and J. C. Hummelen, Adv. Funct. Mater. **11**, 374 (2001).
[12] M. C. Scharber, D. Mühlbacher, M. Koppe, P. Denk, C. Waldauf, A. Heeger, and C. J. Brabec, Adv. Mater. (Weinheim, Ger.) **18**, 789 (2006).
[13] J. L. Brédas, D. Beljonne, V. Coropceanu, and J. Cornil, Chem. Rev. (Washington, D.C.) **104**, 4971 (2004).
[14] X. Cai, M. W. Burand, C. R. Newman, D. A. D. S. Filho, T. M. Pappenfus, M. M. Bader, J. L. Brédas, K. R. Mann, and C. D. Frisbie, J. Phys. Chem. B **110**, 14590 (2006).
[15] T. M. Pappenfus, M. W. Burand, D. E. Janzen, and K. R. Mann, Org. Lett. **5**, 1535 (2003).
[16] K. Schulze, C. Uhrich, R. Schüppel, K. Leo, M. Pfeiffer, E. Brier, E. Reinold, and P. Bäuerle, Adv. Mater. (Weinheim, Ger.) **18**, 2872 (2006).
[17] J. W. Arbogast, A. P. Darmanyan, C. S. Foote, Y. Rubin, F. N. Diederich, M. M. Alvarez, S. J. Anz, and R. L. Whetten, J. Phys. Chem. **95**, 11 (1991).
[18] E. Brier, E. Reinhold, P. Kilickiran, E. Schillrufer, T. Debaerdemaker, M. Pfeiffer, and P. Baeuerle (unpublished).
[19] C. Uhrich, R. Schueppel, A. Petrich, K. Leo, M. Pfeiffer, E. Brier, P. Kilickiran, E. Reinold, and P. Baeuerle, Adv. Funct. Mater. **17**, 2991 (2007).
[20] E. Runge and E. K. U. Gross, Phys. Rev. Lett. **52**, 997 (1984).
[21] E. K. U. Gross and W. Kohn, Adv. Quantum Chem. **21**, 255 (1990).
[22] E. K. U. Gross, J. F. Dobson, and M. Petersilka, Top. Curr. Chem. **181**, 81 (1996).
[23] A. D. Becke, J. Chem. Phys. **98**, 5648 (1993).
[24] A. Schäfer, H. Horn, and R. Ahlrichs, J. Chem. Phys. **97**, 2571 (1992).
[25] R. Bauernschmitt and R. Ahlrichs, Chem. Phys. Lett. **256**, 454 (1997).
[26] F. Furche and R. Ahlrichs, J. Chem. Phys. **117**, 7433 (2002).

[27] see http://www.turbomole.de for current version.
[28] B. W. D'Andrade, S. Datta, S. R. Forrest, P. Djurovich, E. Polikarpov, and M. E. Thompson, Org. Electron. **6**, 11 (2005).
[29] Q. Xie, E. Pérez-Cordero, and L. Echegoyen, J. Am. Chem. Soc. **114**, 3978 (1992).
[30] N. Sato, Y. Saito, and H. Shinohara, Chem. Phys. **162**, 433 (1992).
[31] R. W. Lof, M. A. van Veenendaal, B. Koopmans, H. T. Jonkman, and G. A. Sawatzky, Phys. Rev. Lett. **68**, 3924 (1992).
[32] Q. Xie, F. Arias, and L. Echegoyen, J. Am. Chem. Soc. **115**, 12639 (1993).
[33] J. J. M. Halls, J. Cornil, D. A. dos Santos, R. Silbey, D.-H. Hwang, A. B. Holmes, J. L. Brédas, and R. H. Friend, Phys. Rev. B **60**, 5721 (1999).
[34] J. Gierschner, J. Cornil, and H. Egelhaaf, Adv. Mater. (Weinheim, Ger.) **19**, 173 (2007).
[35] G. Bidan, A. D. Nicola, V. Enée, and S. Guillerez, Chem. Mater. **10**, 1052 (1998).
[36] J. Reimers, Z.-L. Cai, A. Bilic, and N. S. Hush, Ann. N.Y. Acad. Sci. **1006**, 235251 (2003).
[37] T. M. Halasinski, J. L. Weisman, R. Ruiterkamp, T. J. Lee, F. Salama, and M. Head-Gordon, J. Phys. Chem. A **107**, 3660 (2003).
[38] J. Casado, M. Z. Zgierski, R. G. Hicks, D. T. J. Myles, P. Viruela, E. Orti, M. C. R. Delgado, V. Hernandez, and J. T. L. Navarrete, J. Phys. Chem. A **109**, 11275 (2005).
[39] M. Wohlgenannt, X. M. Jiang, and Z. V. Vardeny, Phys. Rev. B **69**, 241204(R) (2004).
[40] V. Wintgens, P. Valat, and F. Garnier, J. Phys. Chem. **98**, 228 (1994).
[41] J. Casado, R. P. Ortiz, M. C. R. Delgado, R. Azumi, R. T. Oakley, V. Hernandez, and J. T. L. Navarrete, Synth. Met. **95**, 93 (1998).
[42] J. J. Apperloo, R. A. J. Janssen, P. R. L. Malenfant, L. Groenendaal, and J. M. J. Frechet, J. Am. Chem. Soc. **122**, 7042 (2000).
[43] S. Rentsch, J. P. Yang, W. Paa, E. Birckner, J. Schiedt, and R. Weinkauf, Phys. Chem. Chem. Phys. **1**, 1707 (1999).
[44] A. Pogantsch, G. Heimel, and E. Zojer, J. Chem. Phys. **117**, 5921 (2002).
[45] C. C. You and F. Wurthner, J. Am. Chem. Soc. **125**, 9716 (2003).
[46] M. A. Greaney and S. M. Gorun, J. Phys. Chem. **95**, 7142 (1991).
[47] J. W. Arbogast, C. S. Foote, and M. Kao, J. Am. Chem. Soc. **114**, 2277 (1992).
[48] D. R. Lawson, D. L. Feldheim, C. A. Foss, P. K. Dorhout, C. M. Elliott, C. R. Martin, and B. Parkinson, J. Electrochem. Soc. **139**, L68 (1992).
[49] M. Baumgarten, A. Gugel, and L. Gherghel, Adv. Mater. (Weinheim, Ger.) **5**, 458 (1993).
[50] L. Biczok, H. Linschitz, and R. I. Walter, Chem. Phys. Lett. **195**, 339 (1992).
[51] R. A. J. Janssen, M. P. T. Christiaans, K. Pakbaz, D. Moses, J. C. Hummelen, and N. S. Sarifciftci, J. Chem. Phys. **102**, 2628 (1995).
[52] Note that the number of double bonds (depicted in Fig. 6) refers to the quinoid structure of D_0 and T_1, i.e., with $N=2n+1$ one double bond less than in the corresponding S_0 structure.
[53] C. Botta, S. Luzzati, R. Tubino, D. D. C. Bradley, and R. H. Friend, Phys. Rev. B **48**, 14809 (1993).
[54] G. Dellepiane, C. Cuniberti, D. Comoretto, G. F. Musso, G. Figari, A. Piaggi, and A. Borghesi, Phys. Rev. B **48**, 7850 (1993).
[55] M. Westerling, C. Vijila, R. Österbacka, and H. Stubb, Synth. Met. **135**, 321 (2003).
[56] R. Schueppel, C. Uhrich, K. Leo, M. Pfeiffer, E. Brier, R. Reinold, and P. Baeuerle, ChemPhysChem **8**, 1497 (2007).
[57] J. J. Apperloo, C. Martineau, P. A. van Hal, J. Roncali, and R. A. J. Janssen, J. Phys. Chem. A **106**, 21 (2002).
[58] T. A. Ford, I. Avilov, D. Beljonne, and N. C. Greenham, Phys. Rev. B **71**, 125212 (2005).
[59] R. Schueppel *et al.*, Proc. SPIE **6656**, 66560G (2007).
[60] D. Veldman, T. Offermans, J. Sweelssen, M. M. Koetse, S. C. J. Meskers, and R. A. J. Janssen, Thin Solid Films **511**, 333 (2006).
[61] D. Veldman, J. J. A. M. Bastiaansen, B. M. W. Langeveld-Voss, J. Sweelssen, M. M. Koetse, S. C. J. Meskers, and R. A. J. Janssen, Thin Solid Films **511**, 581 (2006).
[62] V. I. Arkhipov, P. Heremans, and H. Bässler, Appl. Phys. Lett. **82**, 4605 (2003).
[63] M. Pfeiffer, A. Beyer, T. Fritz, and K. Leo, Appl. Phys. Lett. **73**, 3202 (1998).
[64] B. Maennig, M. Pfeiffer, A. Nollau, X. Zhou, K. Leo, and P. Simon, Phys. Rev. B **64**, 195208 (2001).
[65] J. Drechsel, B. Männig, D. Gebeyehu, M. Pfeiffer, K. Leo, and H. Hoppe, Org. Electron. **5**, 175 (2004).
[66] B. Maennig *et al.*, Appl. Phys. A: Mater. Sci. Process. **79**, 1 (2004).
[67] K. Walzer, B. Maennig, M. Pfeiffer, and K. Leo, Chem. Rev. (Washington, D.C.) **107**, 1233 (2007).
[68] P. Peumans and S. R. Forrest, Appl. Phys. Lett. **79**, 126 (2001).
[69] J. Drechsel, A. Petrich, M. Koch, S. Pfützner, R. Meerheim, S. Scholz, J. Drechsel, K. Walzer, M. Pfeiffer, and K. Leo, SID Int. Symp. Digest Tech. Papers **37**, 1692 (2006).
[70] J. Staudigel, M. Stossel, F. Steuber, and J. Simmerer, J. Appl. Phys. **86**, 3895 (1999).